A Three Dimensional Electrical Model of PEMFC Stack

Mathieu Le Ny, Olivier Chadebec, Gilles Cauffet, Jean-Marc Dedulle, Yann Bultel

A Three Dimensional Electrical Model of PEMFC Stack

M. Le Ny[1,2]*, O. Chadebec[2], G. Cauffet[2], J. M. Dedulle[3], Y. Bultel[1]

[1] Laboratoire d'Electrochimie et de Physico-Chimie des Matériaux et des Interfaces (LEPMI), UMR 5279 CNRS, Grenoble INP, UdS, UJF
[2] Grenoble Electrical Engineering Laboratory (G2Elab), UMR 5269 CNRS, Grenoble-INP, UJF
[3] Laboratoire des Matériaux et du Génie Physique (LMGP), UMR 5628 CNRS, Grenoble-INP

Abstract

Mathematical modeling is an essential tool in the design of fuel cell systems, as it is important to understand the response of a stack under different conditions. This paper proposes a three dimensional electrical model of PEMFC stack. Such approach highlights the phenomena that occur at the macroscopic scale which are the electrical interactions taking place within the stack. At this scale, the microscopic phenomena are taken into account by averaging them over all the thickness of the membrane electrode assembly (MEA). This model consists of solving the charge transport equation in three dimensions. In order to avoid interfacial issues with the potential jump that occurs in the MEAs, a special source term is added in the transport equation. It makes the model robust, reliable, and helpful for understanding the effect of anomalies on the electric behavior of a PEMFC stack. After describing the equations and the numerical method used for the model, the paper shows some electrical phenomena such as cells interactions, non-equipotential bipolar plate, higher cell voltages and internal loop of current.

Keywords: Cell Interaction, Fault Modeling, Internal Loop of Current, PEMFC Stack Modeling

1 Introduction

Proton exchange membrane fuel cells (PEMFC) are energy conversion devices that produce electricity and heat directly from hydrogen and oxygen. Nevertheless, in spite of undeniable progresses undergone both in scientific knowledge and technological development, PEMFC assemblies and parts still present certain drawbacks and improvements must be made such that the system is reliable for industrial applications. Reliability and durability appear to be the most important considerations to successfully achieve the commercialization of proton exchange membrane fuel cell (PEMFC). Fuel cells are prone to chemical, mechanical, or thermal degradation [1] and three degradation classes could be distinguished: "baseline degradation", as well as degradation due to transients and incident induced degradation. All these degradation classes induce fuel cell voltage/performance decrease and lifetime reduction. The baseline degradation is due to long-term material degradation. It is irreversible, unavoidable, and exists as long as the fuel cell is operating. The second and third degradation classes are linked to the variations of operating conditions or detrimental operating conditions. Such degradations are induced by temperature, water management, or under faulty control of operating parameters, such as reactant starvation which refers to an operation with an insufficient amount of gas in the active layer.

In the ideal situation, cells in a stack have to perform uniformly. Unfortunately, this cannot be observed experimentally. The reason for the non-uniform operation of the cells in the stack is still not well understood. Significant variations among the cells may accelerate long-term structural problems and may eventually lead to a total failure of the power generation unit. Possible causes are non-uniform fuel/air flow distribution to individual cells, non-uniform temperature, and current distribution within the stack, and material non-uniformities (compositions and microstructure).

Generally, the modes of membrane electrode assembly (MEA) degradation can be divided in three categories: cata-

[*] *Corresponding author, mathieu.le-ny@g2elab.grenoble-inp.fr*

lyst activity loss, carbon support porosity loss, and membrane conductivity loss. The first is caused primarily by loss of the platinum surface area through dissolution/precipitation platinum during voltage cycling. Additionally, catalyst activity can degrade through poisoning. Damage to the carbon support occurs through corrosion during high potential excursion that is generally caused either by hydrogen-air front on the anode during shutdown/start-up or localized fuel starvation. Finally, it is conceivable that membrane can undergo chemical degradation. All this degradation processes as well as MEA delamination would be manifested as an increase of the MEA resistance. As well as MEA degradation, membrane drying, or electrode flooding can also induce an increase of the cell resistance.

Flow-field channels obstruction by liquid water and fuel cell design anomaly can both induce uneven gas distribution or even local insufficient supply of reactants. Another cause of improper gas supply could be a low reactant flow rate aiming at maximizing reactant utilization in order to optimize fuel cell efficiency. In this situation, coming from oxygen fed in the fuel cell's cathodic compartment (respectively from hydrogen fed in the fuel cell's anodic compartment), oxygen (respectively hydrogen) molecules could diffuse due to the concentration gradient towards the anode (respectively cathode) where they accumulate. In addition to the problem associated with sudden load increase, start-ups and shut-down might be affected by the possible presence of air inside the anodic compartment, particularly after a prolonged shutdown. Finally, in addition to chemical degradation, mechanical degradation of membrane can occur due to water management. Cycling relative humidity causes the membrane to expand and contract by absorbing varying quantities of water. Both chemically and mechanically degraded membrane can induce localized pinhole formation. As a consequence, fuel or oxidant gas starvation and pinhole formation can induce a local decreasing of the electromotive force which can suddenly tend to zero.

PEMFC modeling is a powerful tool in improving the durability and the reliability. In many models, cells are often studied alone, regardless of the surrounding elements. But in reality, cells are integrated in large stacks and interact with their neighbor cells. Up to date, although lot of work has been devoted on single fuel cell modeling, less attention has been paid in the literature to the behavior of a whole fuel cell stack. In Ref. [2], Park et al. describes a 20-cell stack model in which each cell operate uniformly. In order to study the fluidic interactions, Karimi et al. propose a hydraulic network approach in Ref. [3], whereas Burt et al. developed a pseudo 2D model using Finite Volume Method in Ref. [4]. There is also a stack model using partial system approach [5]. In Refs. [6, 7], Gerard et al. present a multi-physic model with a complex 3D discretization of a stack. If some of these models highlight the fluidic and thermal interactions between cells, none of them takes into full account the electrical phenomena. Bipolar plates are not modeled or are considered equipotential. These approaches make impossible the study of many of the electrical interaction that can occur between the cells of a same stack. For diagnostic application and stack stabilization purpose, Hirschfeld et al. [8] developed a 3D electrical model of PEMFC stack using the Finite Volume Method and whose equations in the MEA are more detailed in Ref. [9]. This approach is really useful to see the effects of resistive faults inside a stack and to study the influence of aluminum plates that have stabilization purpose. Nevertheless they do not seem to take into account the potential jump that occurs in the MEAs. Even if this model is capable of predicting the effect of many resistive faults, getting the right potential distribution remains always impossible as well as the phenomena associated to inhomogeneous distribution of electromotive forces. Finally, in Refs. [10, 11], Berg et al. developed a 1 + 1 dimensional electrical and fluidic model of PEMFC stack using their own numerical approach. Currently, it is the more advanced PEMFC stack model taking electrical coupling into account. But its numerical approach makes it difficult to reproduce.

The aim of this paper is to present an electrical model of PEMFC stack that provides the three dimensional steady state distribution of the potential and current density for various cells' configurations and operating conditions. In this model, the electrical phenomena at the stack's level are highlighted instead of the electrochemical and mass transport processes that take place at microscopic scale as it is done usually. The contributions of the anode, the cathode, and the membrane are not distinguished. All the physical phenomena that take place in these different layers are approximated and averaged over the MEA thickness. Fluidic, thermal transfer, and dynamical behavior are not yet taken into account but should be incorporated in our code in future work. The Finite Volume Method is used here because of some of its advantages. This technique allows some modularity with the definition of the problem (geometry, mesh, and physics) and involves only flux balance equations which are equivalent to the Kirchhoff's nodal rule. This makes the model relatively easy and quick to reproduce for someone writing his own code. Moreover, in order to take into account the potential jump that occurs in the MEAs, a special source term in the transport equation is proposed here. This term avoids interfacial issues, can be discretized, integrated, and approximated like any other term in the transport equation and can also be implemented in other numerical method such as the Finite Element Method. Finally the equations presented here can either be solved using a commercial package or using a homemade code. The model presented here is implemented within Matlab with a homemade library of functions that is able to solve problems involving transport equations with the Finite Volume Method.

The Section 2 of this paper presents the equations used for the model. Based on that approach, the electrical behavior of a PEMFC is simulated by considering classical stack geometry and physical parameters as described in Section 3. The model is also used to evaluate the system sensibility to design parameters. In Section 4, simulations are performed to ana-

lyze the impact of MEA anomalies on the electrical characteristics. Phenomena such as cell interactions, non-equipotential bipolar plates, and internal loop of current are highlighted.

2 Formulation

Electrical charges are driven through fuel cells, thanks to complex electrochemical processes that involve many mass and charges transfers. The 3D modeling of these phenomena requires resolutions of many coupled partial differential equations. But here the objective is to model large fuel cells stacks with short time computation. As a consequence resolving coupled partial differential equations at the microscopic level in each MEA of the stack is not suitable. The choice was made to focus on the macroscopic behavior of the stack and to not distinguish the nature of the charge carriers (protons or electrons). An equivalent charge carrier is considered for the whole stack. Mass and heat transfers are not considered yet. This section describes how only one partial differential equation can be chosen in order to compute the 3D steady state macroscopic distribution of current and potential inside a stack. This way of modeling allows the study of the electrical behavior of large stacks with coarse meshes and very efficient time computation.

2.1 Transport Equation in Steady State Current Conduction

The electrical behavior of a stack is based on the equations of electromagnetism. Usually the steady state charge conservation equation and the local Ohm's law are used assuming that the electric field derives from a potential:

$$div\ \mathbf{j} = 0 \tag{1}$$

$$\mathbf{j} = \sigma\ \mathbf{E} \tag{2}$$

$$\mathbf{E} = -\mathbf{grad}\ V \tag{3}$$

where j is the current density, E the electric field, V the potential, and σ the electrical conductivity that can vary according the region of the stack. Combining these three equations leads to the well-known transport equation:

$$\mathrm{div}\,\sigma\,\mathbf{grad}\,V = 0 \tag{4}$$

In PEMFC single cell models, Eq. (4) is generally used to model the transport of some charges in some regions of a cell but it is not used for all the charge carriers in all regions. Here the objective is to consider only one charge carrier and to have only one equation for the whole stack. But if Eq. (4) is used alone, it cannot take into account energy sources inside a volume. With this kind of formulation, energy sources can only be introduced via the boundary conditions. It is a problem here because the energy comes from the fuel cell itself and not from the exterior. This energy source is related to the potential jump induced by the electrochemical phenomena occurring in the Membrane Electrode Assembly (MEA). In consequence, an additional term related to the electrochemical behavior of the MEA needs to be added, so Eq. (4) can be used as a stand alone equation for the whole stack.

2.2 Addition of an Electromotive Force Term in the Transport Equation

In the previous section, the electrical field was assumed to derive from a potential. But it is not always true and the electrical field can be written in a more general form:

$$\mathbf{E} = \mathbf{E_m} - \mathbf{grad}\ V \tag{5}$$

where E_m is the electromotive field. This term allows the modeling of a force that can drive charges through a medium. In stacks this force arises because of the electrochemical phenomena occurring inside the MEA. In this paper, this term will be often referred as the electromotive force. The reason is that the electromotive field is the electromotive force per unit length. Using again Eqs. (1) and (2), the new charge transport Eq. (6) includes now an additional term. Thanks to this known source term, the electrical behavior of a stack can be easily modeled with a set of two distributions parameters: the conductivity and the electromotive field.

$$div\ \sigma\ \mathbf{grad}\ V - div\ \sigma\ \mathbf{E_m} = 0 \tag{6}$$

The electromotive field is null inside bipolar plates and end plates. Its value in the MEA is the open circuit voltage (OCV) divided by the thickness of the MEA in the linear case.

2.3 Addition of Materials With Non-Linear Behavior

For sake of simplicity, our approach was previously developed in the case of a linear behavior for the fuel cell. Nevertheless, it is well known that a PEMFC exhibits a non-linear electrochemical behavior. This response can be characterized by a MEA's polarization curve resulting from a model or from experimental measurement. In this paper, an empirical polarization curve of the form (7) was chosen:

$$\Delta V(j) = U_\mathrm{mo} - R_\mathrm{so} j - A \ln\left(\frac{j}{j_\mathrm{eq}} + 1\right) \tag{7}$$

where U_mo is the OCV of one cell, R_so the total resistance of the MEA and A and j_eq are fitted parameters that represent the activation overpotential due to electrochemical reactions. The analytical function (7) is a source of information that models the behavior of MEAs. A Newton–Raphson algorithm was used to couple this equation with Eq. (6) in MEA regions. The procedure is presented in the annex.

3 PEMFC Stack Model

In this section, equations presented previously are used to model a PEMFC stack. An overview of the model is given by describing the geometry and by giving an example of param-

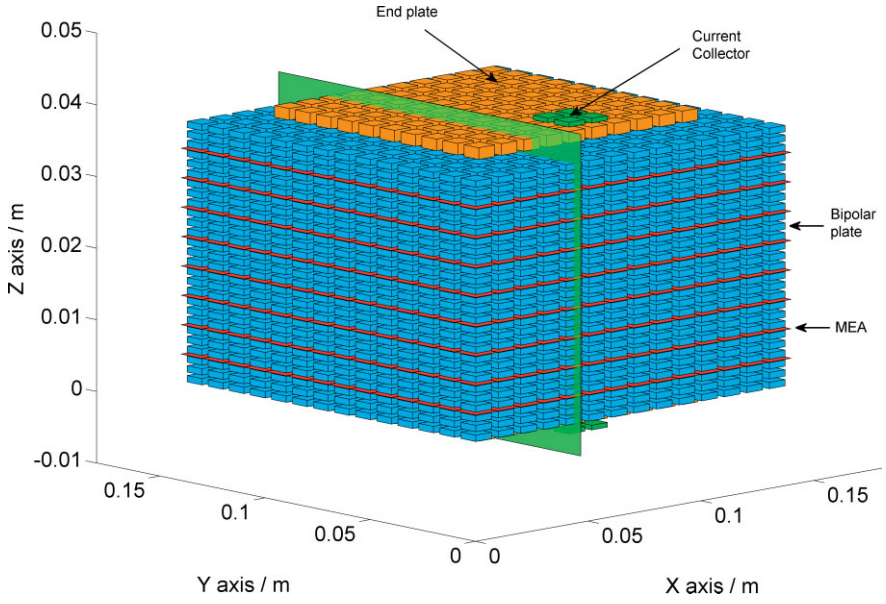

Fig. 1 3D view of PEMFC stack's geometry and mesh with the localization of a cross section (green).

eter distribution in the situation of a healthy behavior. This can be done by assuming a uniform gas concentration distribution through the stack. This means that the oxygen and hydrogen gas concentration is constant along the gas channel. These operations conditions are achieved when the stochiometric coefficient is larger than the unity or the reactant utilization is very low.

3.1 Geometry, Mesh, and Physic

This model is built up of multiple single repeat units stacked on top of each other and sandwiched between two end plates along the z-axis. In Figure 1, each color represents a physical region with different parameters. In the examples shown in this paper, the stack consists of eight cells and the current collecting was considered to be performed on the edge of the PEMFC stack. It is important to remind that there is only one region for all the thickness of a MEA. The cathode, the anode and the membrane are not distinguished. All the physical phenomena that take place in these different layers are averaged over the MEA thickness and represented by the local polarization law. Finally, different kind of boundary conditions can be used at the terminal of the stack. In order to control the stack with voltage or with current or with a load, Dirichlet, Neumann or Robin conditions are respectively used.

In order to reduce the size of the mesh, surface elements were used for all the MEA regions. As a consequence, transverse currents in MEA are considered null. Currents can use transverse paths only in bipolar plates or in end plates. With the mesh shown in Figure 1 simulations are performed within a few seconds. Results of simulations are not sensitive to the mesh density along the z-axis and a coarser mesh can be used if simulations have to be performed on a stack with a large number of cells. The mesh density chosen in the x- and y-directions gives an error inferior to 2%.

3.2 PEMFC Stack Parameters

Table 1 gives the parameters values used for each region in the case of a healthy fuel cell stack. For sake of simplicity, a linear polarization law can be first considered to simulate the electrical behavior of the stack. For a MEA, we consider an OCV for single cell equal to 0.9 V and an effective MEA conductivity equal to 5 S m^{-1} (Table 2).

Using a linear behavior for MEAs is a good approximation if what is needed is the study of the mechanisms that explain the cells interactions. If accurate results are desired, a more complex polarization law for MEA can be used like the one given in Eq. (2.5) and whose parameters are given in Table 3.

Table 1 Stack parameters.

Current collector conductivity	$5\ 10^7$ S m^{-1}
End plate conductivity	$5\ 10^7$ S m^{-1}
Bipolar plate conductivity	$5\ 10^3$ S m^{-1}
Current collector thickness	1 mm
End plate thickness	2.5 mm
Bipolar plate thickness	4 mm
MEA thickness	0.1 mm
Current collector area	0.02 × 0.02 m^2
End plate area	0.14 × 0.14 m^2
Bipolar plate surface area	0.14 × 0.14 m^2
MEA surface area	0.1 × 0.1 m^2

Table 2 Parameters used for a MEA for linear polarization law (healthy PEMFC stack).

MEA electromotive force (U_{m0})	0.9 V
MEA resistance per unit area (R_{s0})	$2\ 10^{-5}$ Ω m^{-2}

Table 3 Parameters used for a MEA for non-linear polarization law (healthy PEMFC stack).

MEA electromotive force (U_{m0})	1 V
MEA resistance per unit area (R_{s0})	1.79 10^{-5} Ω m^2
MEA non-linear parameter (A)	0.025 V
MEA non-linear parameter (j_{eq})	90 A m^{-2}

The parameters given here correspond to a stack fed with pure oxygen and composed of graphite bipolar plate.

3.3 Electric Behavior of a Healthy PEMFC Stack

The next figures present the electrical behavior of healthy PEMFC stacks considering the standard parameters (Table 1). The Figure 2 presents the simulated stack voltage versus the current flowing through the stack for the both cases of linear and non-linear electrochemical behaviors. The Figures 3a–c presents the current density and cell voltage distribution through the PEMFC stack. Simulation is performed considering a current equal to 100 A flowing through the stack. The current goes from the lower potential to the higher potential and not the opposite as in passive materials. This is due to the electromotive force term added in the transport equation. As the gas phase distribution is not taken into account, homogeneous distributions are observed whatever the current collector position is. The distribution of the streamlines through a cross section (see Figure 3c) shows that the larger end plate conductivity allows the redistribution of the current. It is worth mentioning that the seal on the edge of the cells induce a curvature of the streamlines. For sake of simplicity, the simulated results are obtained for the case of a linear behavior. Note that similar results are recorded when considering a non-linear law.

This PEMFC stack model is able to investigate the effects of material properties and design parameter on the stack's operating conditions. For example if a material with a conductivity of 10^4 S m^{-1} is chosen for the end plate, Figure 4 shows what would be the effect of such choice on the electrical behavior of the stack. Similar results are obtained if the thickness of the end plates is decreased by two orders of magnitude. In this case, heterogeneous cell voltage and current density distributions are recorded. Due to cell-to-cell electrical coupling, each cell has a slightly different electrical behavior. The highest current densities and lowest cell voltages are shown close to the external current collector (Figures 4a,b). The cells in the middle of the stack demonstrate the smoothest behavior. As expected, the distribution of the streamlines (Figure 4c) shows that the lower end plate conductivity allows only partly the redistribution of the current. In consequence, the positioning of the current collector can impact the current density and potential distribution when considering lower end plate conductivity.

4 Electric Behavior of a Faulty PEMFC Stack

The simulations results described in this section are performed to predict the change in current density and potential through the stack taking into account anomalies into the PEMFC stack. The main capability of this model is the possi-

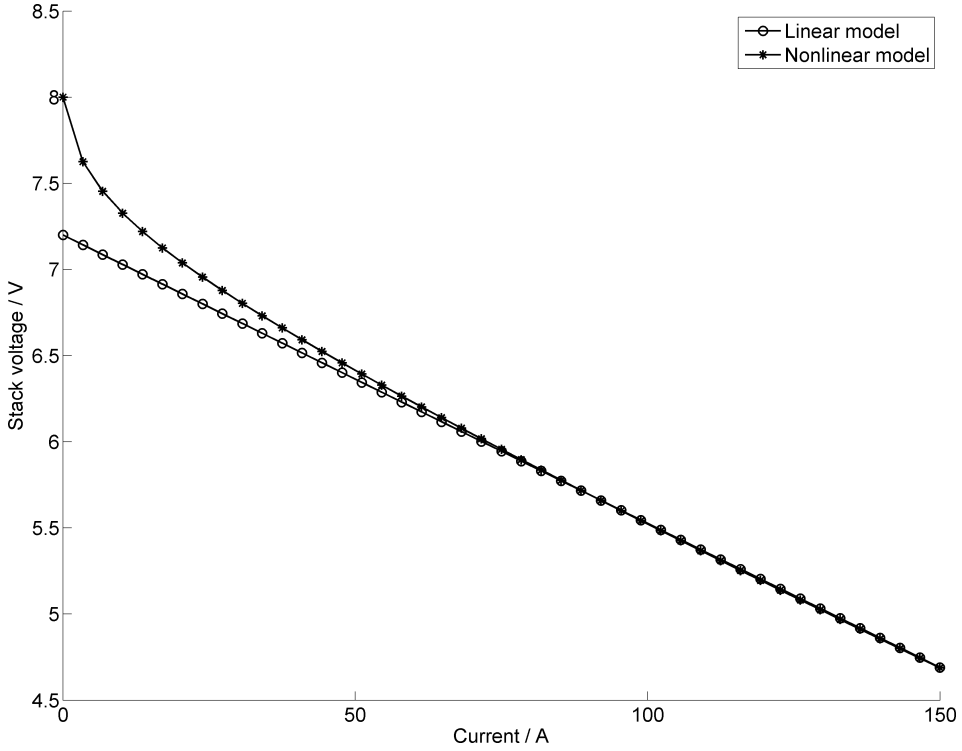

Fig. 2 Stack voltage versus current curves for the PEMFC stack: linear (○) and non-linear (*) electrochemical behaviors.

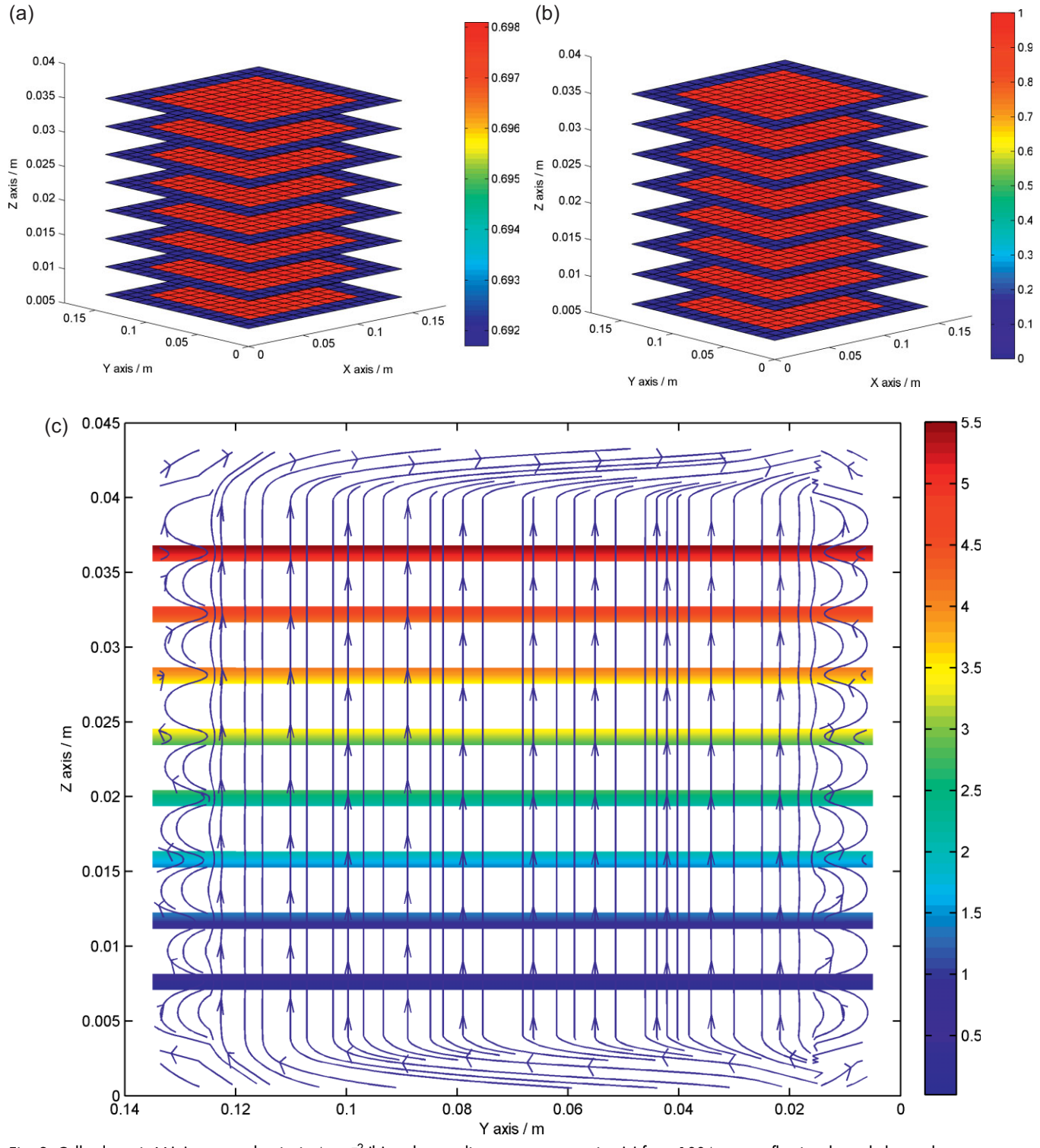

Fig. 3 Cell voltage in V (a), current density in A cm^{-2} (b) and streamlines on a cross section (c) for a 100A current flowing through the stack.

bility to induce inhomogeneous distribution of electrochemical parameters. This technique of modeling allows the computation of the effects of inhomogeneous distribution of conductivities and electromotive forces. Membrane dehydration, water flooding as well as materials degradation are assumed to generate a MEA resistance increase. Conversely, reactant crossover and starvation can induced a decay of the electromotive force. The Figure 5 then presents the position of the induced anomalous resistance and anomalous OCV. We consider an arbitrary MEA conductivity four times lower for the

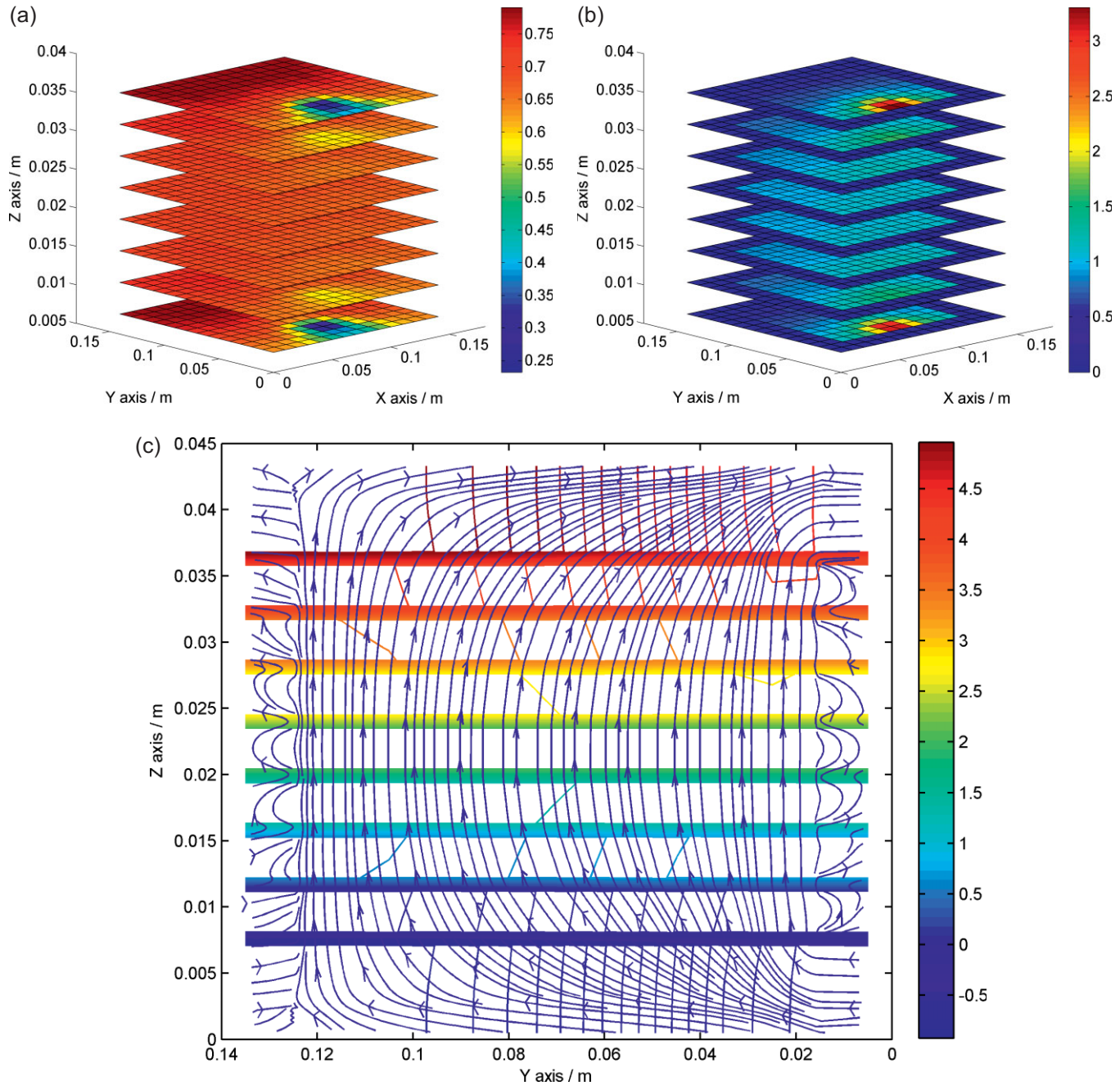

Fig. 4 Cell voltage in V (a), current density in A cm^{-2} (b) and streamlines on a cross section (c) for a 100A current flowing through the stack: case of lower end plate conductivity (10^4 S m^{-1}).

first case and a OCV close to zero in the second case on one corner of the cell number 6. The last case considers the transient distribution of OCV (Figure 5c) during fuel cell shutdown or start-up when ambient air may be introduced or removed in the anode gas channels, respectively.

This section presents the electrical behavior of a faulty PEMFC stack by considering these two types of anomalous and their consequences on the potential, current and performances. First, the Figure 6 provides the voltage stack versus current when considering either the resistive anomalies (Figure 5a) or the anomalous electromotive force (Figure 5b). The global effect of these two kinds of anomaly is highlighted by comparison to the case of the healthy stack. As expect, the slope of voltage stack versus current curve increases when considering an anomalous resistance meanwhile the OCV of the stack shift toward lower value in the case of an anomalous electromotive force.

4.1 Anomalous Resistance

In order to illustrate the impact of an anomalous resistance on the electrical behavior (Figure 5a), Figure 7 shows the

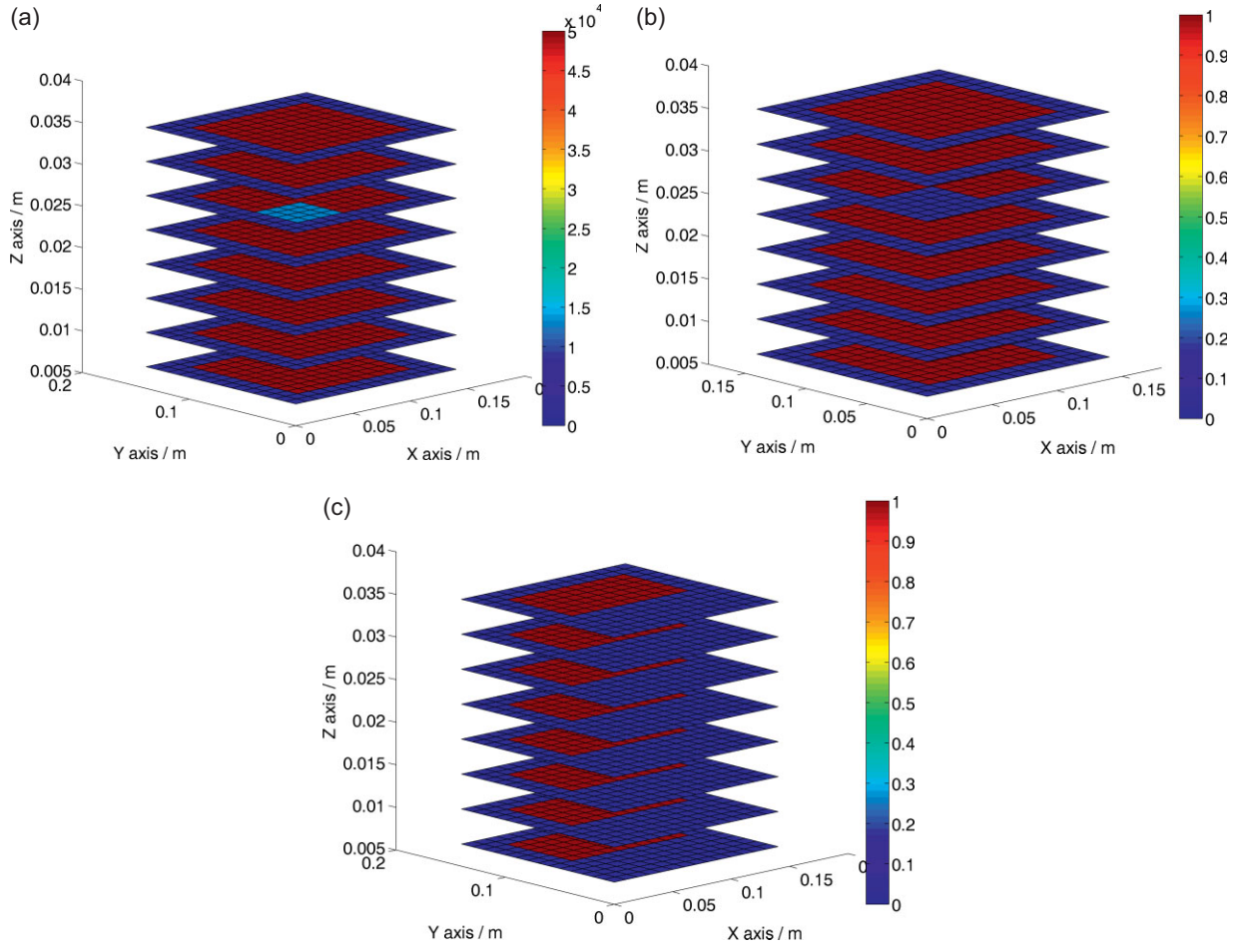

Fig. 5 Anomalous distribution of conductance (in S m^{-2}) (a) and anomalous distribution of OCV (in V) (b) on one corner of the sixth cell. Anomalous distribution of OCV (in V) on the lower part of all cells (c).

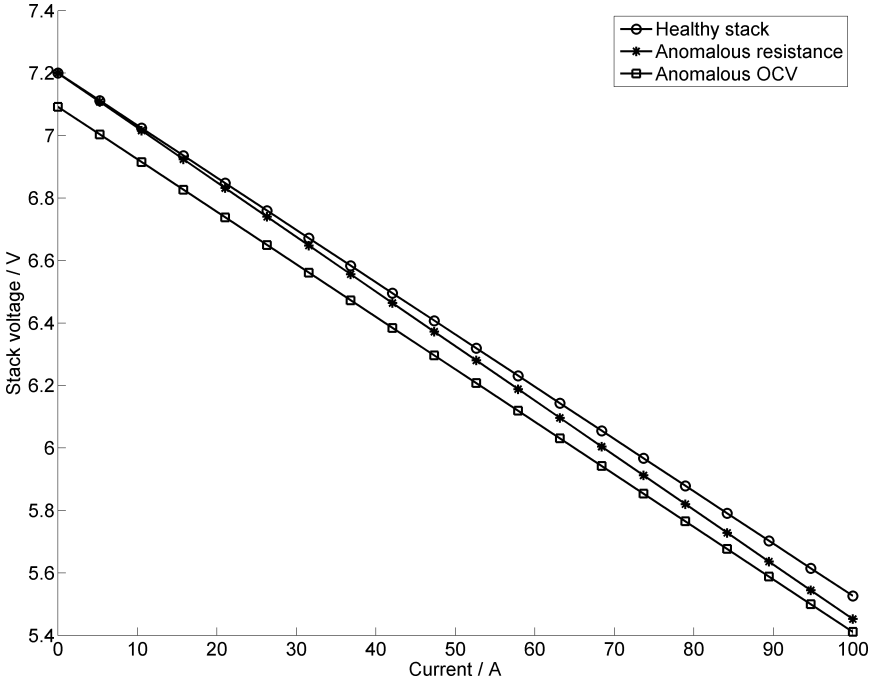

Fig. 6 Voltage stack versus current curve obtained in case of a healthy behavior (o), in the case of an anomalous resistance (+) and in the case of an anomalous OCV (□).

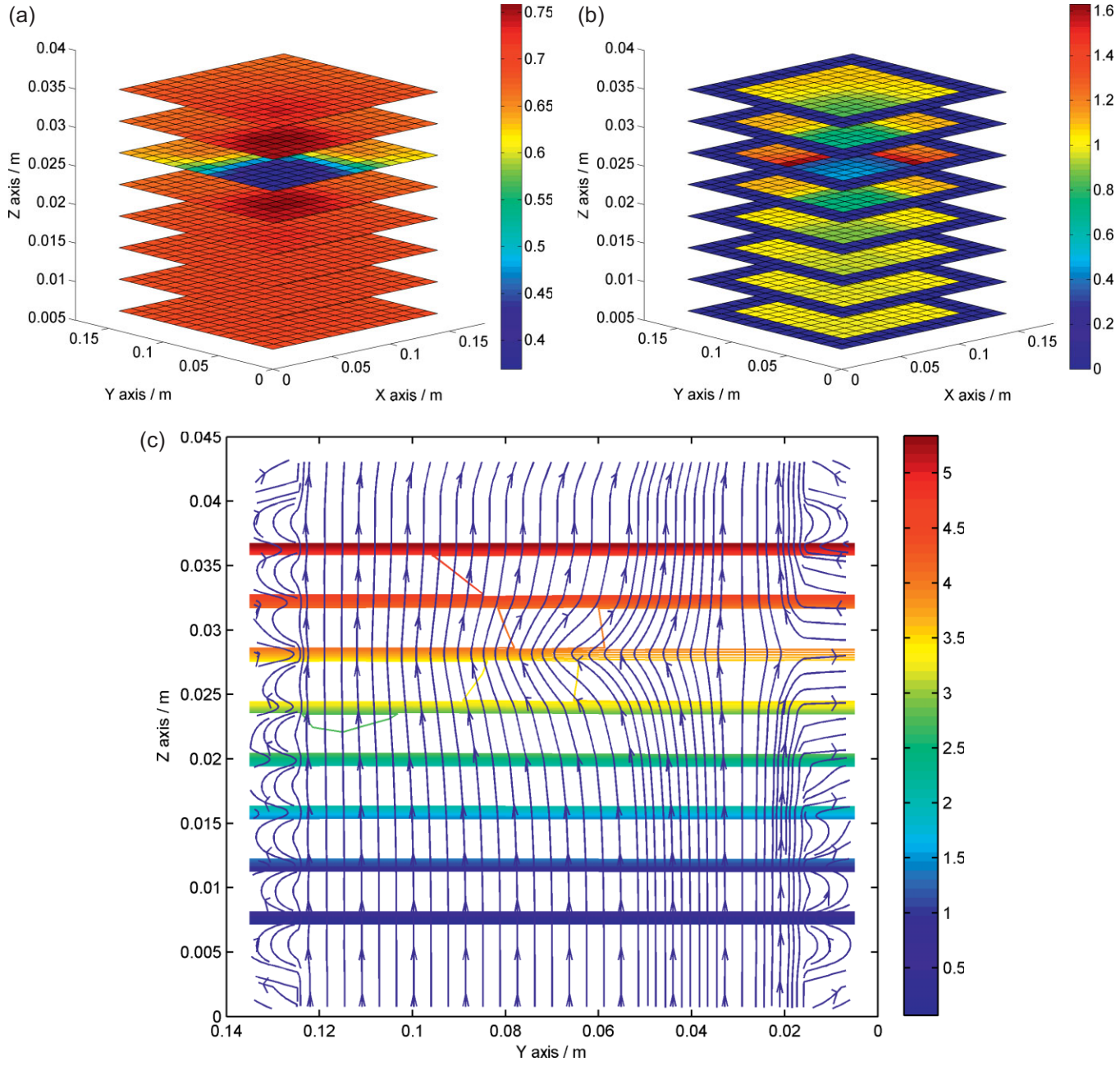

Fig. 7 Cell voltage in V (a), current density in A cm^{-2} (b) and streamlines on a cross section (c) for a 100A current flowing through the stack: case of anomalous resistance.

simulated cell voltage, current density and streamlines distribution through the PEMFC stack. The significant effect of the non-uniform resistance of the cell 6 is demonstrated. The both current density and cell voltage distributions (Figure 7a,b) are highly modified to force the current to pass through the healthy part of the cell 6. As it can be seen on Figure 7, this anomaly partially blocks the current flowing through the anomalous zone and induces low cell voltage. Conversely, this redistribution induces largest current densities close to the anomalous zone. Such behavior certainly causes hot spot in vicinity of the anomaly. The faulty cell 6 is severely affected but neighboring cells 5 and 7 are also impacted due to cell-to-cell electrical coupling. In consequence, healthy cells can suffer from inhomogeneous current due to a neighbor defective cell. Namely, fifth and seventh cells exhibit lower current densities and higher cell voltages close to the anomalous zone. Nevertheless, it is worth mentioning that the importance of this coupling between cells heavily depends on two parameters. When both conductivity and the thickness of the bipolar plate increase, the importance of the coupling decreases. In consequence the importance of cell interactions will heavily depend on the technology used for the PEMFC.

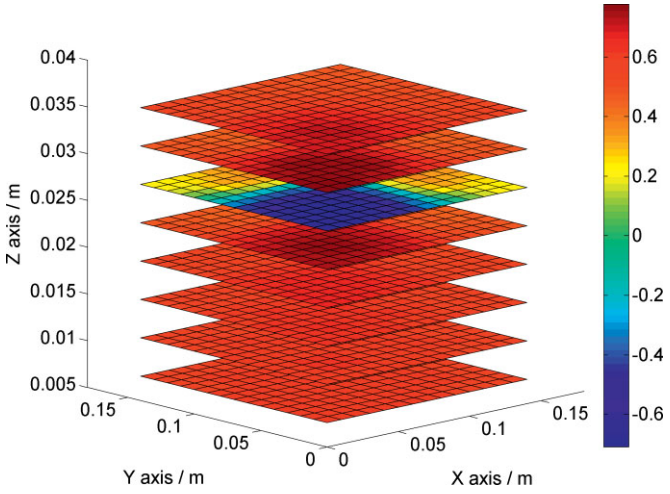

Fig. 8 Cell voltage distribution for a 150 A current flowing through the stack with a larger anomalous resistance.

The streamlines (Figure 7c) highlight another electrical phenomenon. This anomalous resistance partially blocks the current in the main direction and forces it to use transverse paths. These transverse currents create voltage drops inside a same bipolar plate which is not anymore equipotential. The figure shows that equipotential lines are bent out. These variations of potential on a same bipolar plate can reach about tens or hundreds millivolts depending on the current flowing through the stack and the bipolar plate material conductivity.

Finally, it is important to note that the neighbor's cells (cells 5 and 7) exhibit higher cell voltages close to the anomalous resistance (Figure 7a). These higher values have two explanations: the voltage drop created by the transverse currents in bipolar plates and a lower ohmic drop in AME regions with less current flowing through. As a consequence the healthy cells located close to anomalies can suffer from accelerating degradation processes such as carbon corrosion and platinum dissolution due to these induced higher cell voltages. This effect of anomalous resistance was already investigated in Refs. [12–15]. The results presented here are consistent with the ones shown in these papers.

In Figure 7a, the voltage of the sixth cell at the bottom is very low but still positive. Larger anomalous resistance can induce negative voltage, over a part of the cell or on the entire cell (Figure 8). This phenomenon occurs when the surface of the fault becomes too much important or if the conductivity of the anomalous zone becomes very low. In fact, a one dimensional model is enough to explain the phenomenon of negative voltage cell. The voltage of one cell is equal to the electromotive force of the cell minus the ohmic drop term. If resistance of the cell increases too much, the ohmic drop term becomes higher than the electromotive force term and the voltage of the cell becomes negative.

4.2 Anomalous Gas Phase Distribution

Figure 9 shows simulations performed with a local electromotive force (or OCV) assumed equal to zero at the bottom of the sixth cell (Figure 5b). The significant effect of a non-uniform gas distribution in the cell 6 is demonstrated. The both current density and cell voltage distributions are highly modified. The cell voltages exhibit lower values (Figure 9a) over the anomalous region meanwhile the current densities present negative values (Figure 9b). When few current is allowed to leave out the stack, the high electromotive force in the healthy region of cell 6 push the charge through area with lower electromotive force. The consequence here is this induced internal loop of current on the sixth cell (Figure 9c).

These simulations were performed using a MEA's linear response that allows currents in the opposite direction. So it has to be reminded that electrochemical non-linearity mainly hold back this phenomenon. Thus, the backward currents computed here are entirely over evaluated. But if the model is modified so that no reverse current is allowed, the results show that an electric field in the opposite direction remains in the anomalous region. This electric field produces a force that tries to move the charges backwards. If electrochemical processes allow some kind of charge transfer, a few current might flow in the opposite direction. The question about how much current will really flow backwards is beyond the scope of this paper. The point we want to emphasize here is that simple steady state electrical considerations can lead to configurations that create forces that try to push the charges in the opposite direction.

This behavior could be explained by the reverse current decay mechanism proposed by Reiser et al. [16] in the case of fuel starvation associated to improper gas supply. Because of the oxygen permeation through the membrane, oxygen reduction occurs at the anode meanwhile either oxygen evolution or carbon corrosion potentially occurs at the cathode. At the anode, electrons are then provided by the healthy part for oxygen reduction due to the transverse current whereas the healthy part of the cathode are partly fed by electrons coming from the faulty part of the cathode. Similar electrochemical behavior might be proposed in the case of oxidant starvation. This model predicts that the anodic regions filled with oxygen might create locally favorable reverse-current conditions in these exposed regions. The created reverse-current might cause local cathode degradation.

The model also shows that internal loops of current are amplified when considering a stack under reactive gases at the OCV (Figure 10). It also shows that if internal loops of currents exist (whatever are their origins), cells close to the anomaly have voltages higher than the OCV. The phenomenon is quite similar to the one encountered with anomalous resistance. As in this previous case, the transverse currents flowing in the bipolar plates create voltage drops that induce higher cell voltages on the neighboring cells. But here no current is flowing through the membrane of these healthy cells, so the local total voltage can become higher than the OCV.

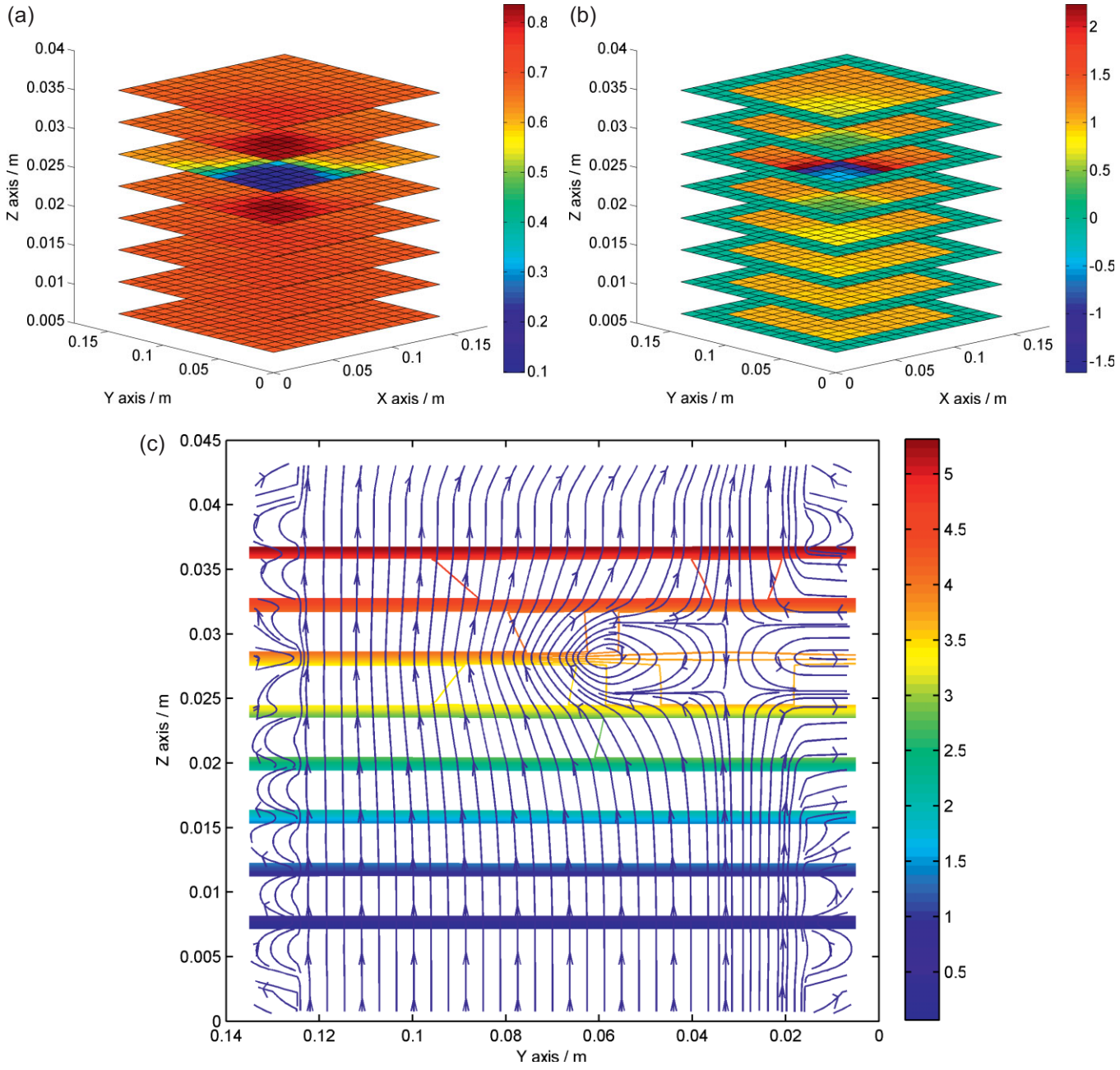

Fig. 9 Cell voltage in V (a) current density in A cm^{-2} (b) and streamlines on a cross section (c) for a 100 A current flowing through the stack: case of anomalous OCV.

This means that these healthy cells can also suffer from accelerating carbon corrosion and platinum dissolution due to these higher cell voltages.

Unbalanced electromotive forces can also be encountered during shutdown or start-up. When a fuel cell is shutdown, ambient air may introduce in the anode gas channels where it replaces hydrogen. Conversely, during start-up, a transient fuel–air front is created along anode gas channels. In the both case, the anode catalyst layer is subjected to localized or even complete fuel starvation. When hydrogen pushes the air that was introduced to purge the stack (or respectively air pushes the hydrogen), there is a brief instant when a part of the MEA is subjected to an electromotive force while an other part is not. In consequence, this inhomogeneity creates an internal loop of current involving all the cells of the stack (Figure 11). Lastly it has to be reminded that other phenomena like the discharge of double layer capacity [17] can also contribute to reverse currents and mask this phenomenon.

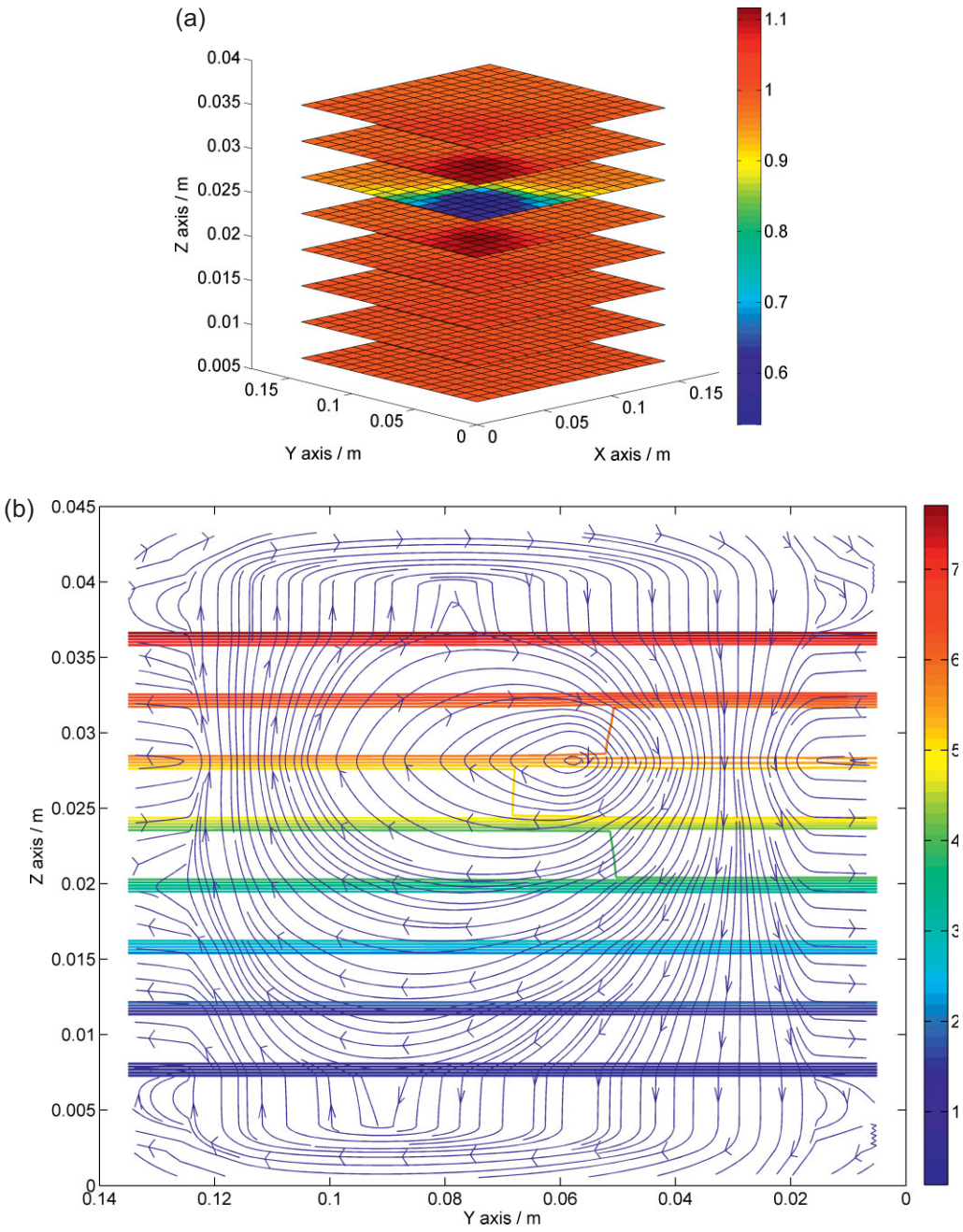

Fig. 10 Cell voltages (a) and streamlines on a cross section (b) for a 0 A current flowing through the stack in the case of an anomalous OCV.

5 Conclusion and Perspectives

A 3D electrical model for PEMFC has been developed in order to provide a tool that quickly evaluates potential and current density distributions in stacks with very large numbers of cells. The addition of a special source term in the charge transport equation allows the macroscopic modeling of stacks considering only one equivalent charge carrier. The model was found to be useful to analyze the influence of stack parameters, operation conditions, and perturbations. The model is robust, fast, easy to implement, and allows the study of electrical phenomena such as the mechanism of cell interactions, non-equipotential bipolar plates, higher cell voltages, or internal loop of current. The results of simulations indicate that the variations in local current density and cell potential among cells in a stack are strongly influenced by the electrical properties of materials and the stack geometry. Moreover, cell-to-cell variations can occur partially due to anomalies within the stacks of cells. It is shown that the effects of electrical coupling on the stack behavior are quite significant.

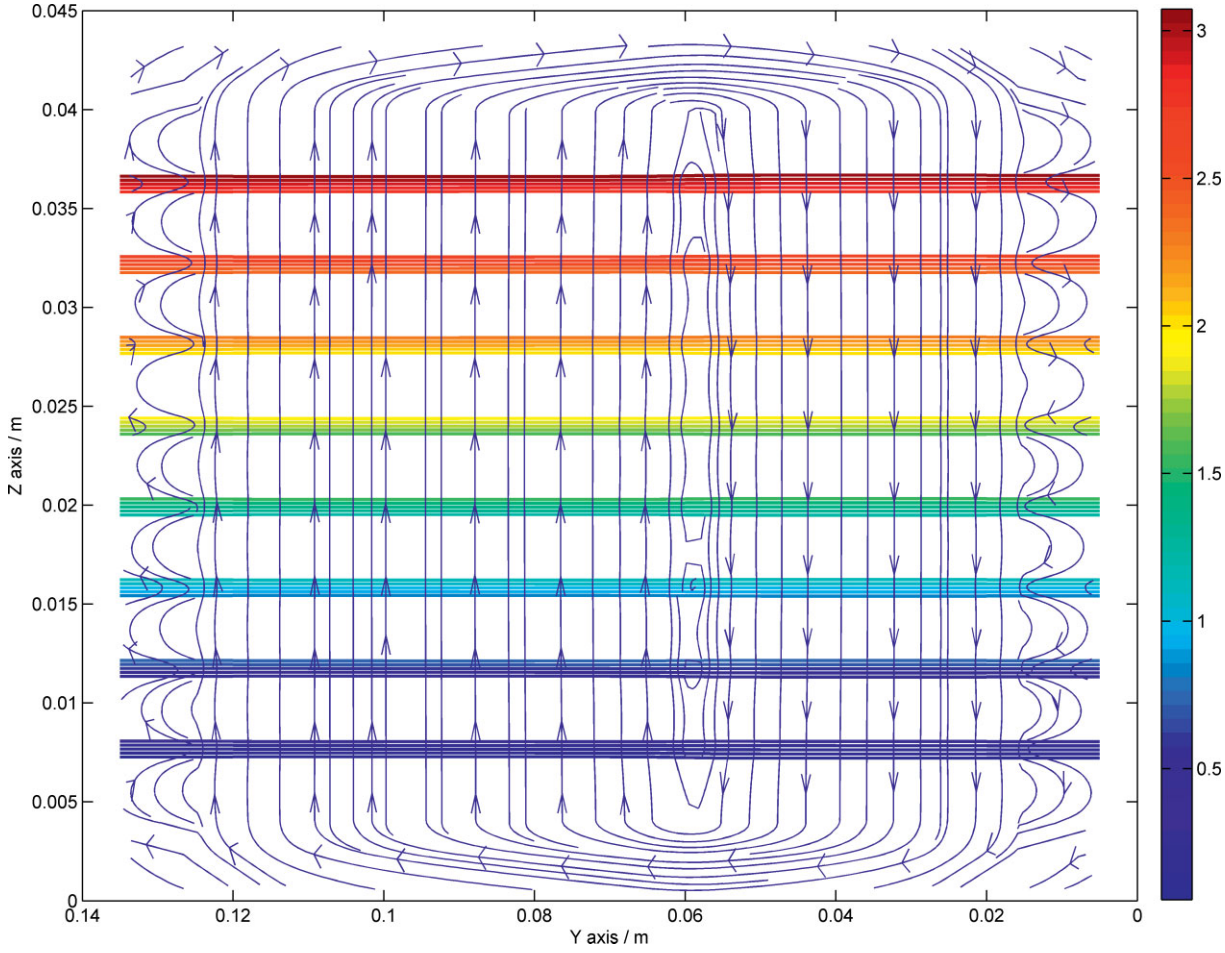

Fig. 11 Streamlines on a cross section during start-up or shutdown operations (0 A of total current).

Acknowledgment

The authors thank the Agence Nationale de la Recherche (ANR) for their financial support as well as the partners of the OMNISCIENTS project: PSA Peugeot Citroën, Helion, Commissariat à l'Energie Atomique et aux Energies Alternatives (CEA) and Euro Physical Acoustics (EPA).

Annex: Non-Linear electrochemical behavior of MEA

This annex describes how the differential Eq. (A.1) used to model the electrical behavior of a stack is coupled with a polarization law (Eq. A.2) that takes into account the non-linear response of the MEA. This approach is based on a Newton–Raphson algorithm that consists on linearizing an equation around some points until convergence is reached. The procedure given here can be used on any polarization law similar to Eq. (A.2) as far as derivation and convergence is possible.

$$div\ \sigma\ \mathbf{grad}\ V - div\ \sigma\ \mathbf{E_m} = 0 \tag{A.1}$$

$$\Delta V(j) = U_{\mathrm{mo}} - R_{\mathrm{so}} j - A \ln\left(\frac{j}{j_{\mathrm{eq}}} + 1\right) \tag{A.2}$$

Eq. (A.1) was obtained using the following general form of the local Ohm's law:

$$\mathbf{j} = \sigma\ \mathbf{E_m} - \sigma\ \mathbf{grad}\ V \tag{A.3}$$

The Ohm's law can also be written using global variables.

$$\Delta V = U_{\mathrm{m}} - R_{\mathrm{s}} j \tag{A.4}$$

If parameters are considered constants over the thickness t_{MEA} of the MEA, the relations between local and global parameters can be written using Eq. (A.5).

$$\begin{cases} \sigma \approx \dfrac{t_{\mathrm{MEA}}}{R_{\mathrm{s}}} \\ E_{\mathrm{mz}} \approx \dfrac{U_{\mathrm{m}}}{t_{\mathrm{MEA}}} \end{cases} \tag{A.5}$$

while Eq. (A.2) is non-linear, it is possible to state that it can be linearized around some point j_n using a Taylor expansion of the first order.

$$\Delta V(j) \approx \Delta V(j_n) + (j - j_n)\frac{\partial \Delta V}{\partial j}(j_n) \tag{A.6}$$

By identifying Eq. (A.4) with Eq. (A.6), the electromotive force and resistance per unit area around some point j_n can be defined by Eq. (A.7):

$$\begin{cases} R_s(j_n) = -\dfrac{\partial \Delta V}{\partial j}(j_n) \\ U_m(j_n) = \Delta V(j_n) - j_n \dfrac{\partial \Delta V}{\partial j}(j_n) \end{cases} \tag{A.7}$$

Using Eq. (A.2) and Eq. (A.7), it is possible to get analytical functions that give the variations of the resistance and electromotive force with the current density.

$$\begin{cases} R_s(j_n) = R_{so} + A\dfrac{1}{j_n + j_{ex}} \\ U_m(j_n) = U_{mo} - A\ln\left(\dfrac{j_n}{j_{ex}} + 1\right) + j_n A\dfrac{1}{j_n + j_{ex}} \end{cases} \tag{A.8}$$

Eq. (A.1) is then solved iteratively using the parameters given by Eq. (A.8) and Eq. (A.5) at each iteration until convergence is reached.

References

[1] N. Yousfi-Steiner, Ph. Moçotéguy, D. Candusso, D. Hissel, *J. Power Sources* **2009**, *194*, 130.

[2] S.-K. Park, S.-Y. Choe, *J. Power Sources* **2008**, *179*, 660.

[3] G. Karimi, J. J. Baschuk, X. Li, *J. Power Sources* **2005**, *147*, 162.

[4] A. C. Burt, I. B. Celik, R. S. Gemmenb, A. V. Smirnov, *J. Power Sources* **2004**, *126*, 76.

[5] J. H. Lee, T. R. Lalk, *J. Power Sources* **1998**, *73*, 229.

[6] M. Gerard, J.-P. Poirot-Crouvezier, P. Schott, D. Hissel, M.-C. Pera, *Proceeding of FDFC Conference Nancy*, **2008**.

[7] M. Gerard, J.-P. Poirot-Crouvezier, D. Hissel, M.-C. Pera, *Int. J. Hydrogen Energ.* **2010**, *35*, 12295.

[8] J. Hirschfeld, H. Lustfeld, M. Reißel, B. Steffen, *Int. J. Energ. Res.* **2009**, *34*, 293.

[9] H. Lustfeld, M. Reißel, B. Steffen, *Fuel Cells* **2009**, *4*, 474.

[10] P. Berg, A. Caglar, K. Promislow, J. St-Pierre, B. Wetton, *IMA J. Appl. Math* **2006**, *71*, 241.

[11] P. Chang, G. S. Kim, K. Promislow, B. Wetton, *J. Comput. Phys.* **2007**, *223*, 797.

[12] M. Santis, S. A. Freunberger, M. Papra, A. Wokaun, F. N. Büchi, *J. Power Sources* **2006**, *161*, 1076.

[13] S. A. Freunberger, I. A. Schneider, P. C. Sui, A. Wokaun, N. Djilali, F. N. Büchi, *J. Electrochem. Soc.* **2008**, *155*, B704.

[14] A. A. Kulikovsky, *J. Electrochem. Soc.* **2007**, *154*, B817.

[15] Y. Bultel, L. Gautier, M. Zahid, P. Stevens, J. M. Klein, *ECTS Trans.* **2007**, *7*, 1791.

[16] C. A. Reiser, L. Bregoli, T. W. Patterson, J. S. Yi, J. D. Yang, M. L. Perry, T. D. Jarvi, *Eletrochem. Solid-State Lett.* **2005**, *8*, A273.

[17] G. Maranzana, C. Moyne, J. Dillet, S. Didierjean, O. Lottin, *J. Power Sources* **2010**, *195*, 5990.